Two-Dimensional Aeroelastic Analysis of a Brimmed-Diffuser Shroud with Composite Material for a Wind Turbine

Taeyoung Kim[+1], Hiroto Nagai[+2], Kousei Ono[+2], Nobuhide Uda[+2] and Yuji Ohya[+3]
[+1]Dept. of Aeronautics and Astronautics, Grad School of Engineering, Kyushu Univ., Fukuoka, Japan
[+2]Dept. of Aeronautics and Astronautics, Faculty of Engineering, Kyushu Univ., Fukuoka, Japan
[+3]Research Institute for Applied Mechanics, Kyushu Univ., Fukuoka, Japan

A brimmed-diffuser shroud also known as a wind-lens is equipment to amplify output power in a wind turbine system by collecting and accelerating wind blowing through its rotor area. A small increase in wind speed accelerated by a wind-lens greatly raises output power from a wind power generator because output power is proportional to wind speed cubed. In spite of this advantage, its thin structure is prone to aeroelastic deformation and vibration. Especially, for a large-sized wind-lens, its wind resistance is also required to improve. In this study, aeroelastic response of the two dimensional brimmed-diffuser shroud for a 100kW wind power generator is computed under uniform wind conditions by using a two-dimensional Navier-Stokes code coupled with the equation of motion for the structure. Three types of material were applied to a diffuser model: aluminum alloy, CFRP laminate and sandwich structure with CFRP layers and PET foam. The density of the sandwich structure is lowest among the three materials. The weight of the three models is kept same by adjusting their thickness for analysis, and the model of the sandwich structure has become thickest. We verified that resonance occurs in the models when a vortex frequency matches a natural frequency of the structure. Besides, we confirmed that vibrating motion in resonance depends on a dominant mode shape. As a result, the sandwich model has the least vibrating motion in resonance because of high rigidity by its thickness. Considering the results, our estimation of critical wind speed using a Strouhal number is found to agree well with the aeroelastic responses.

Keyword: Aeroelasticity, Vortex-induced Vibration, Wind-lens, Wind Turbine, Composite Material

1. INTRODUCTION

Figure 1: A wind generator with a brimmed diffuser

A brimmed diffuser shroud is a ring-like device that amplifies output power in a wind power generator[1)]. It is installed around a rotor with a few struts that fix it to a nacelle as seen in Fig. 1. It is also known as a wind-lens because it collects and accelerates wind passing through the rotor area. In addition, it helps passive yaw

[+1]kim-ty@aero.kyushu-u.ac.jp, [+2]nagai@aero.kyushu-u.ac.jp, [+3]ohya@riam.kyushu-u.ac.jp

control of a rotor, so the rotor area can always face a wind direction at all times. With wind speed increased by a wind-lens, a rotor is able to rotate fast, which enables a wind turbine system to gain more output power. Even slightly accelerated wind speed can make a large amount of power because output power is proportional to wind speed cubed. In practice, power generated from a wind power generator with a wind-lens is more than twice as large as that from a conventional one[2]. It is obvious that a brimmed diffuser shroud is advantageous to a wind turbine system in terms of wind energy generation. However, it increases wind load and total weight of a wind power generator by adding it around the rotor. Besides, thin diffuser is exposed to hazardous aeroelastic deformation and vibration in its structure by strong wind. In general, a wind power generator stops its operation over a wind speed of 25 m/s for the safety of a rotor[3]. Even if a rotor remains at rest under the strong wind condition, a wind-lens around the rotor needs to endure gales. In order to design a large and light brimmed-diffuser shroud which is strong enough to be utilized at fast wind speed, this study investigates the aeroelastic influence on its structure made of composite material under uniform wind conditions.

2. NUMERICAL METHODS

(1) Structural model

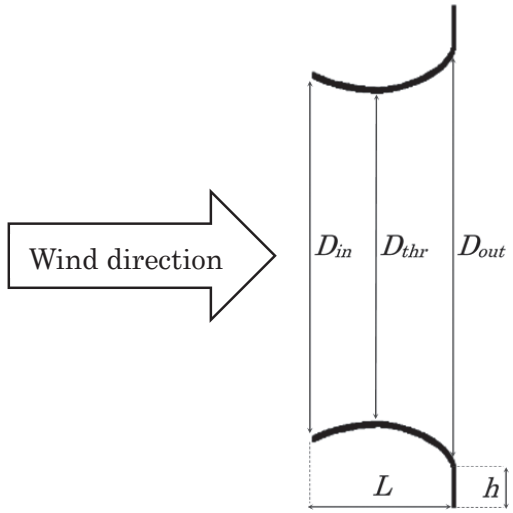

Figure 2: Schematic diagram of a wind-lens model

Table 1: Size of the model

Inlet diameter	D_{in}	15.9m
Throat diameter	D_{thr}	15.6m
Outlet diameter	D_{out}	17.0m
Brim height	h	0.78m
Diffuser length	L	2.14m

A wind-lens for a 100kW generator is the object of this study, illustrated in Fig. 2 and Tab. 1. The brimmed-diffuser named CiB5 consists of a cycloidal curve in the diffuser and a brim with the height of 5% of the throat diameter. The material of a wind-lens in general use is aluminum alloy. We supposed aluminum alloy can be replaced with composite material with CFRP or PET foam to lighten a wind-lens with high stiffness. The material properties of them are as follows.

Table 2: Material properties of CFRP, PET foam, and aluminum alloy

		CFRP ply (0.25mm thick)	PET foam	Aluminum alloy
Young's modulus	E_1	130 GPa	85 MPa	72 GPa
	$E_2,\ E_3$	6 GPa		
Poisson' ratio	$\nu_{12},\ \nu_{13},\ \nu_{23}$	0.33	0.37	0.3
Shear modulus	$G_{12},\ G_{13}$	4 GPa	21 MPa	28 GPa
	G_{23}	2.3 GPa		
Density	ρ	1600 kg/m^3	105 kg/m^3	2700 kg/m^3

Three types of a model were considered by using the three materials above: an aluminum alloy model, a CFRP laminate model, and a model of a sandwich structure which is fabricated as a three-layered structure by attaching

two thin skins to a thick core. In the sandwich model, CFRP laminates are used for both upper and lower faces and PET foam is filled as a core between them. For comparison, the thickness of the diffuser models was adjusted so that all of them can have the same weight.

Table 3: Three types of model

	Material		Total thickness
Aluminum alloy model	Aluminum alloy		6.1mm
CFRP laminate model	CFRP laminate $[(0/90)_{20}/\bar{0}]_s$		10.25mm
Sandwich model	Face: CFRP $[(0/90)_3/0/\overline{90}]_s$ Thickness: 3.75mm each	Core: PET foam Thickness: 42.5mm	50mm

From the Tab. 3, it is clear that the sandwich model has the lowest density. In the layup sequence of the CFRP laminates, 0° direction heads for the axial direction in the cylindrical coordinate of the brimmed-diffuser and 90° direction corresponds with the circumferential direction of that. It is assumed that a wind-lens is fixed by 3 supports at 120° intervals as shown in Fig. 3. The model focuses on the wind-lens only and excludes other parts such as a rotor and a nacelle. For simplification, a diffuser model is cut in sixths as described in Fig. 4.

Figure 3: A brimmed diffuser shroud fixed by 3 supports

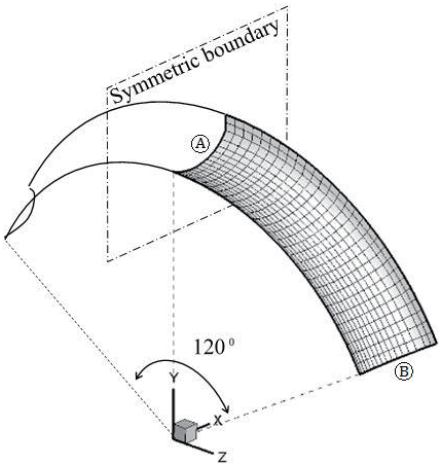

Figure 4: A one-sixth model

(2) Modal analysis

As a first stage, modal analysis of the three abovementioned models was conducted by using a commercial FEM software, ANSYS 15.0, to calculate their mode shapes and natural frequencies. In this FEM analysis, 4-node shell elements were applied for the one-sixth diffuser model. Symmetric boundary conditions were applied at both the sides of A and B in Fig. 4. The side B is additionally fixed and does not move at all in the x-direction (axial direction) since it is supported by a strut. Six modes were obtained in this three-dimensional analysis. Then the 3D mode shapes were reduced to the two-dimensional mode shapes for two-dimensional aeroelastic analysis. Thus, the cross-section of the diffuser model on the symmetric boundary plane (the side A in Fig. 4) is set as the reference cross-section. The first and second mode shapes of the three models are shown in Fig. 5. A natural frequency is a parameter for estimating a resonance phenomenon between a structure and a vortex flow around a diffuser model. In Tab. 4, the sandwich model has the larger natural frequencies than the other models in each mode. In other words, it is most resistant to wind load among them. Figure 5 shows that the first mode of the aluminum alloy model and CFRP laminate model is vibration of the brim, while that for the sandwich model is rotating motion about the circumferential axis at a certain nodal point on the reference cross-section. The second mode shape of the aluminum alloy model and the CFRP laminate

model is vibration of the camber or bending of the shape, while that of the sandwich model is rotating motion about the circumferential axis, which is similar to its first mode shape. The higher-order mode shapes were also obtained, but they do not have a great influence upon aeroelastic responses.

Table 4: The natural frequencies from the first mode to the sixth mode [Unit: Hz]

	f_1	f_2	f_3	f_4	f_5	f_6
Aluminum alloy model	3.38	5.36	6.11	7.46	7.76	9.43
CFRP laminate model	4.33	7.82	9.40	11.91	13.10	14.30
Sandwich model	7.09	13.89	24.56	34.93	40.21	42.22

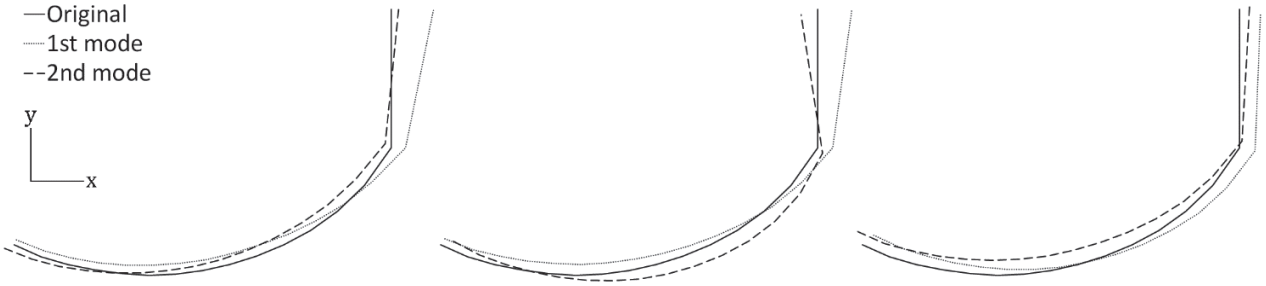

(a) Aluminum alloy model (b) CFRP laminate model (c) Sandwich model

Figure 5: The first and second mode shapes of the cross-section on the symmetric boundary plane

(3) Two-dimensional aeroelastic analysis

We employed a computational fluid dynamics (CFD) developed by Nagai et al. for numerical aeroelastic analysis, which includes a two-dimensional Navier-Stokes code coupled with the equation of motion for the structural model[4)5)]. The modal characteristics from the FEM analysis were used as input data for the CFD program. Based on mode superposition, the displacement vector d_i on the reference cross-section is expressed as

$$d_i(\xi,t) = \sum_{k=1}^{N} \Phi_{ik}(\xi) q_k(t) \qquad (i = 1\sim3,\ k = 1\sim N) \quad (1)$$

where t is time, ξ is the curvature coordinate along the cross-section, q_k is the generalized coordinate of k-th mode, and Φ_{ik} is the natural mode shapes of k-th mode in i-th coordinate direction. N is the number of modes, which is six as mentioned above. Next, Lagrange's equations of motion give us the ordinary equations of motion for $q_k(t)$ as below.

$$M_k\left(\ddot{q_k} + g_k\omega_k\dot{q_k} + \omega_k^2 q_k\right) = \int_{L.E}^{T.E} \Phi_{ik}(\xi)\cdot\Delta P_i(\xi,t)d\xi \qquad (i = 1\sim3,\ k = 1\sim N) \quad (2)$$

In Eq. 2, M_k is the generalized mass, g_k is the modal damping coefficient (= 0.01), ω_k is the natural frequency, and ΔP_i is the pressure difference vector acting on the cross section. ΔP_i is computed at each time step using the 2D Navier-Stokes code absent from turbulence model. If Eq. 2 is solved by numerical time integration, we can gain the generalized coordinate at each time step, and then the deformation of the cross-section using superposition of modes is also determined.

3. RESULTS AND DISCUSSION

(1) Estimation of critical wind speed

The shape of the brimmed-diffuser shroud generates large vortex shedding behind the brim. Although the vortex shedding helps an increase of the flow velocity inside the diffuser, it applies a time-varied aerodynamic load onto the diffuser surface, which may cause severe aeroelastic vibration at a particular wind

speed. The critical wind speed is defined as the wind speed at which the frequency of vortex shedding behind a diffuser model matches one of the natural frequencies of its structure. As the wind speed gets faster, the vortex frequency increases linearly. When the wind speed reaches the critical wind speed, resonance typically arises in an oscillating body by vortices. The Strouhal number St is defined as

$$St = \frac{f_\omega l}{U_0} \tag{3}$$

where f_ω is the vortex frequency, l is the reference length that is vertical distance from the throat to the top of the brim, and U_0 is the wind speed.

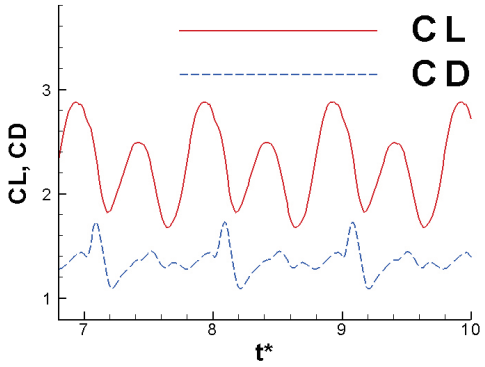

Figure 6: Time history of lift and drag coefficients in the rigid diffuser model

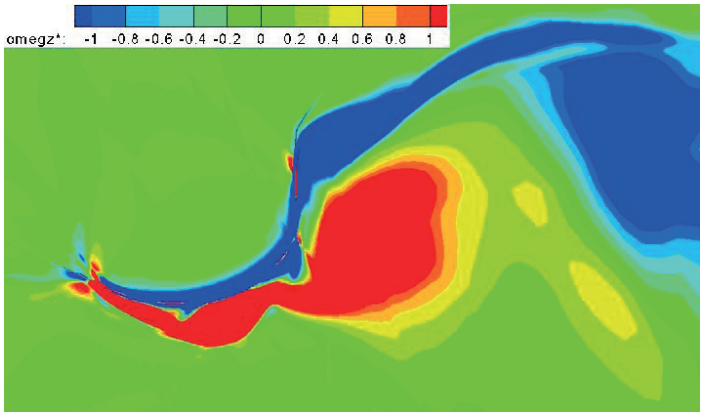

Figure 7: Vortices around the diffuser in the rigid diffuser model

Table 5: Estimated critical wind speeds by the three Strouhal numbers [Unit: Hz]

	Natural frequency [Hz]		Estimated critical wind speed [m/s]		
			St_1=0.063	St_2=0.126	St_3=0.189
Aluminum alloy model	1st mode	3.38	79.3	39.7	26.4
	2nd mode	5.36	125.9	62.9	42.0
CFRP laminate model	1st mode	4.32	101.5	50.8	33.8
	2nd mode	7.82	183.6	91.8	61.2
Sandwich model	1st mode	7.09	166.6	83.3	55.5
	2nd mode	13.89	326.3	163.2	108.8

Firstly, we analyzed a rigid diffuser model at a wind speed of 10m/s with the CFD program to find the Strouhal number for the diffuser shape. The time history of lift and drag coefficients is shown in Fig. 6. Using these waveforms, we calculated the Strouhal number by measuring the wave period. As shown in Fig. 6, the waveform of the aerodynamic force includes some fundamental sinusoidal waves. Each fundamental wave signifies each vortex-shedding frequency as shown in Fig. 7. The Shrouhal number calculated by the lowest vortex frequency is denoted by St_1, which is related to the vortex shedding at the trailing edge of the brim. The Strouhal number St_2 comes from the second lowest vortex frequency which means the vortex shedding inside the diffuser behind the throat. The third Strouhal number St_3 is to do with the vortex shedding around the corner between the diffuser and brim. It possesses a small amplitude and short period within the time history of drag coefficient. In this case, St_1 is 0.063, St_2 is 0.126, twice as much as St_1, and St_3 is 0.189, triple as much as St_1. Once St_i is found, we can estimate the vortex frequency $f_{\omega i}$ at each wind speed. The estimated critical wind speed was calculated from the assumption that the resonance occur when the vortex frequency $f_{\omega i}$ is equal to the structural natural frequency f_{si}. Combining the two natural frequencies with the three Strouhal numbers, we

calculated six estimated critical wind speeds tabulated in Tab. 5. The critical wind speed about the third natural frequency is too high to happen in nature. For this reason, the higher-order natural frequencies were not taken into account in the estimation as well. In this study, we are aiming at a diffuser model that satisfies the designed wind speed limit, 70m/s, and the sandwich model is expected to be suitable for that requirement in the estimation of the critical wind speed.

(2) Aeroelastic response for the aluminum alloy model

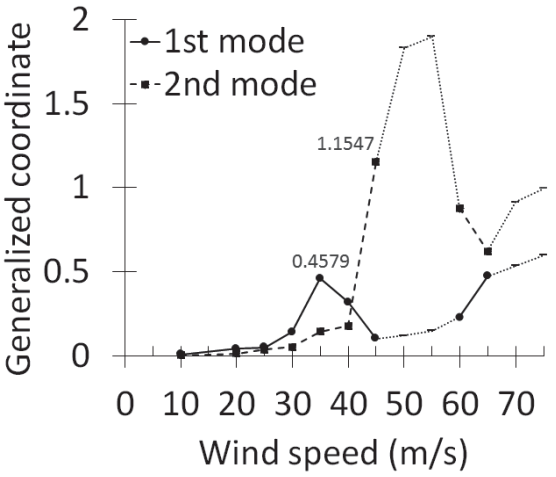

Figure 8: Amplitude of generalized coordinate *vs* wind speed for the aluminum alloy model

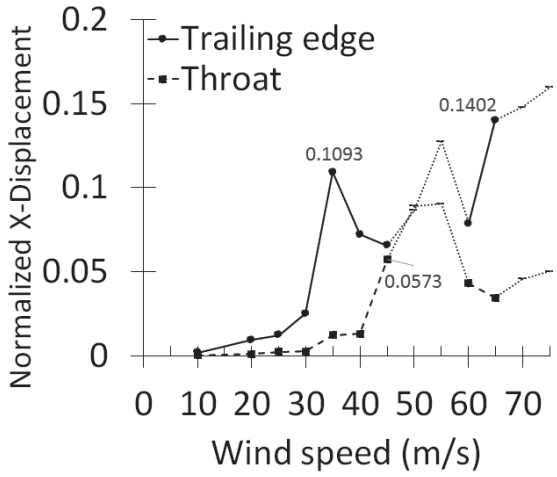

Figure 9: Amplitude of x-displacement *vs* wind speed for the aluminum alloy model

The aeroelastic responses of the aluminum alloy model were calculated under constant flow conditions. Figure 8 shows the amplitude of the generalized coordinates normalized by the diffuser length, L, for the first and second modes with respect to the wind speed. We could not obtain converged data at 50m/s, 55m/s and more than 70m/s and marked (-) signs because the limitation of the CFD grid system when large deformation occurs. In Fig. 8, the first mode has a peak point at 35m/s, which is close to the estimated critical wind speed of 39.7m/s. At this point, the diffuser model has resonance between the second vortex frequency and the first natural frequency. In the second mode, the largest value lies at 45m/s in the second mode. We guess that the peak point of the second mode would appear at 55m/s without the limitation of computation and it would approximately coincide with the estimated critical wind speed of 62.9m/s. The calculated peak points shown in Fig.8 are slightly different from the estimated critical wind speed shown in Tab. 5. This is because the large deformation of the model affects the flow field around the diffuser considerably, which may lead to the change of the vortex frequencies that have already been estimated. Figure 9 shows the amplitude of the deformation normalized by L at the trailing edge of the brim and the throat. It makes sense that the trailing edge is very easy to move in the x-direction since it is subjected to high wind load and the brim moves in all the modes as shown in Fig. 5. The displacement of the trailing edge has a peak point at 35m/s. At more than 40m/s, the displacement of the throat is sharply increased as the second mode becomes dominant. Meanwhile, we could not observe any peak in Fig. 8 and 9 at around 26.4m/s, the critical wind speed about the first natural frequency and the third Strouhal number. The reason is that the intensity of the third vortex shedding is too small to have an effect on the model at such a low wind speed. However, there is an increasing tendency of the second mode from 30m/s to 40m/s in Fig. 8. It indicates that the third vortex shedding whose frequency is close to the natural frequency of the second mode is effective on the deformation at 42m/s, comparatively high wind speed. Figure 10 and 11 show the time histories of the displacement in the x-direction at the trailing edge and the throat at 35m/s and 55m/s. The response of the model at 35m/s shows the resonance phenomenon between the second vortex frequency and the first natural frequency and forms almost in-phase oscillation between the large displacement of the trailing edge and the small displacement of the throat. It is apparent that they are moving together in the

same direction because of the first mode shape as shown in Fig. 5(a). On the other hand, when the second mode is excited at 55m/s, as shown in Fig. 5, vibration of the camber that bends the shape of the diffuser gives rise to the large displacement of the throat moving in the opposite direction to the trailing edge. That is likely to do harm to the structure due to fatigue by the cyclic load. Therefore, the aluminum alloy model underwent resonance in its structure at a wind speed under 70m/s and its deformation at 70m/s is anticipated to be greatly large.

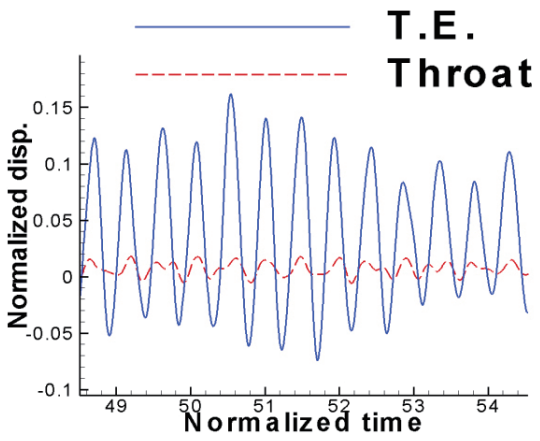

Figure 10: Time history of x-displacement at *U*=35m/s for the aluminum alloy model

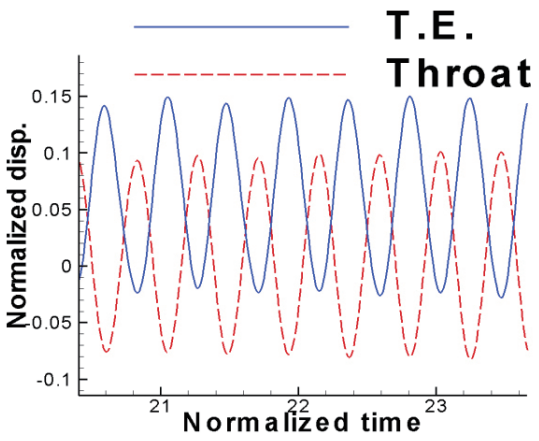

Figure 11: Time history of x-displacement at *U*=55m/s for the aluminum alloy model

(3) Aeroelastic response for the CFRP laminate model

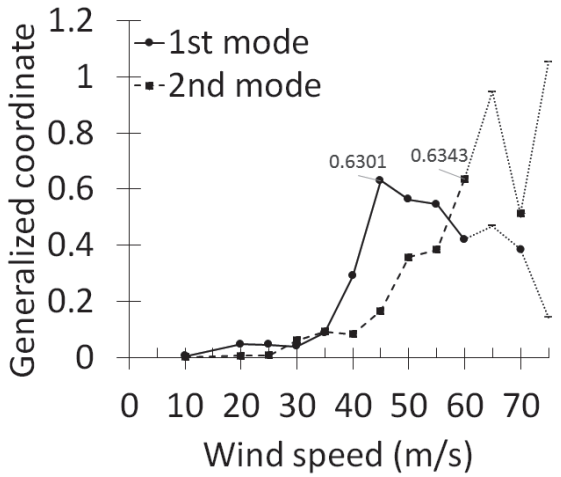

Figure 12: Amplitude of generalized coordinate *vs* wind speed for the CFRP laminate model

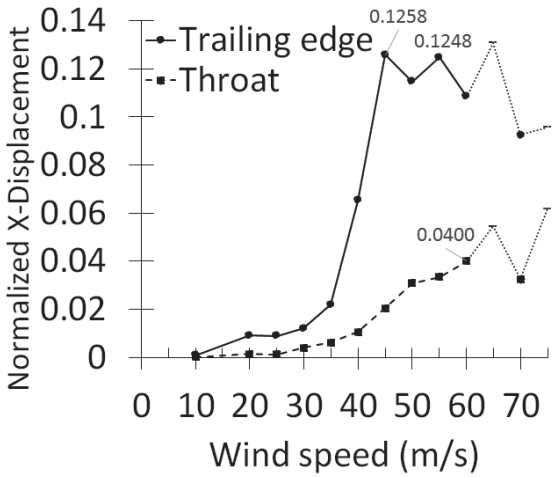

Figure 13: Amplitude of x-displacement *vs* wind speed for the CFRP laminate model

Figure 12 shows the amplitude of the normalized generalized coordinates for the CFRP laminate model with respect to the wind speed. In this graph, a peak point in the first mode appears at 45m/s and it is located near the estimated critical wind speed by the second vortex frequency in the first mode, 50.8m/s. And the second mode is increasing until 60m/s. The computation of the CFD program at 65m/s which is near to the estimated critical wind speed by St_3 in the second mode, 61.2m/s, could not be completed for the same reason with the case of the aluminum alloy model. Thus, the third vortex frequency quite impacted on the diffuser model in this case. Figure 13 shows two peak points at 45m/s and 55m/s in the displacement of the trailing edge and both have almost the same displacement. We assumed that the peak point at 55m/s was caused by a coupling effect of the first mode and the second mode. As shown in Tab. 5, the estimated critical wind speed by St_2 in the first

mode and that by St_3 in the second mode do not have a great difference. That is, the structure of the model has the high possibility of being simultaneously affected by the two kinds of vortex at between the two critical wind speeds. Figure 14 shows the behavior of resonance between the second vortex frequency and the natural frequency of the first mode at 45m/s. Like Fig. 10, the two wave forms are in-phase oscillation with the very large displacement of the trailing edge and the small displacement of the throat. Irregular patterns in Fig. 15 describe the coupling motion of the first mode and the second mode at 55m/s. Some anti-phase patterns between the trailing edge and the throat demonstrate that the second mode is getting strong as wind speed increases. And then, when the second mode becomes dominant, vibration of the camber comes to be remarkable as shown in Fig. 16, which resembles Fig. 11. Similarly, this sort of movement in a wind-lens may deteriorate its fatigue performance in the structure. Comparing to the aluminum alloy model, the first resonance phenomenon in the CFRP laminate model occurs at relatively high wind speed. However, it proved to have considerable displacement in the model at a wind speed over 45m/s although its thickness is larger than that of the aluminum alloy model.

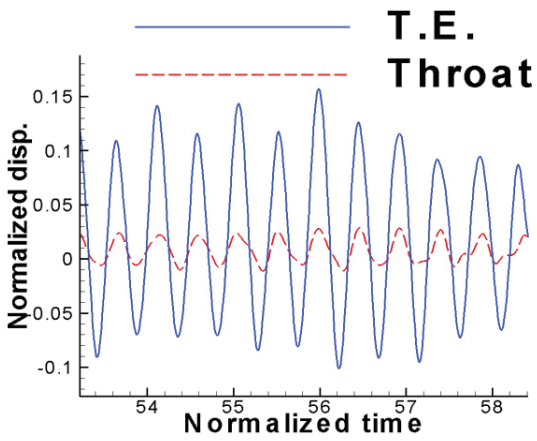

Figure 14: Time history of x-displacement at *U*=45m/s for the CFRP laminate model

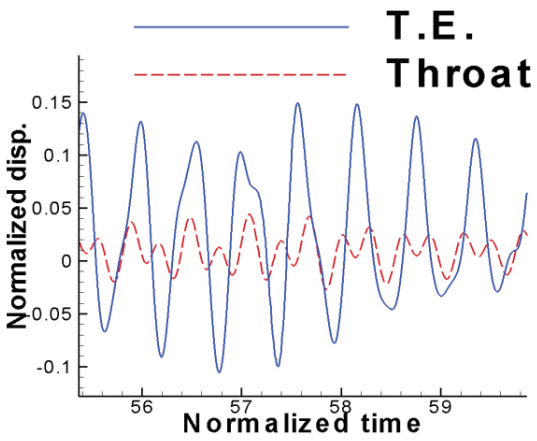

Figure 15: Time history of x-displacement at *U*=55m/s for the CFRP laminate model

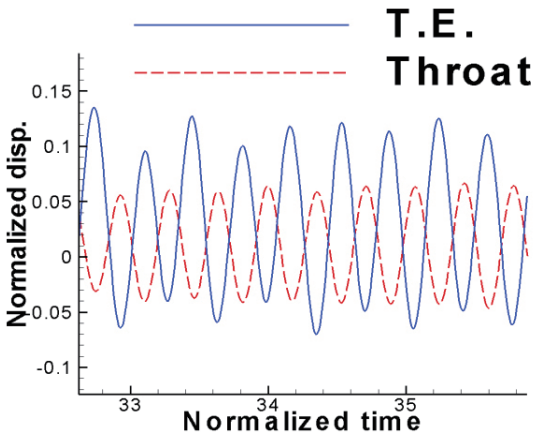

Figure 16: Time history of x-displacement at *U*=65m/s for the CFRP laminate model

(4) Aeroelastic response for the Sandwich model

In both Fig. 17 and 18, it is significant that a maximum value of the vertical axis on the two graphs is much smaller than that of the previous models and no calculation failed for all wind speeds until 75m/s. In the sandwich model, as shown in Tab. 5, the critical wind speed by St_3 in the first mode is estimated to be 55.5m/s and the others predicted are over 70m/s, the designed wind speed limit. Accordingly, there is a peak point at

55m/s in the amplitude of generalized coordinate of the first mode. In the second mode, a noticeable peak point is not seen, but it simply tends to gradually increase. Nevertheless, the other peak point in the first mode appear at 40m/s in Fig. 17. The displacement of the trailing edge in Fig. 18 also has two peak points like Fig. 17. We suppose that the increasing curves after 65m/s in both Fig. 17 and 18 is merely on the way to the critical wind speed by St_2 in the first mode, 83.3m/s, and the one at 40m/s might be influenced by the fourth vortex which has not been identified yet in Fig. 6 and 7. In order to figure out vortices in detail at each wind speed, we are going to employ fast Fourier transform afterward.

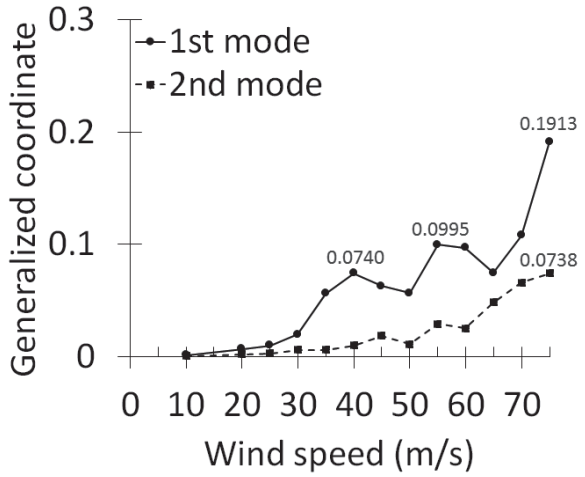

Figure 17: Amplitude of generalized coordinate *vs* wind speed for the sandwich model

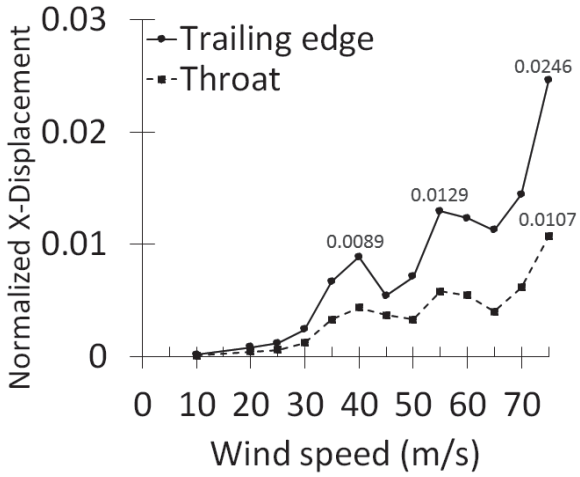

Figure 18: Amplitude of x-displacement *vs* wind speed for the sandwich model

In the three figures from Fig. 19 to Fig. 21, what has in common is their in-phase oscillation between the trailing edge and the throat because the first mode is more dominant than the second mode at all the wind speeds until 75m/s according to Fig. 17. Furthermore, the second mode does not include bending motion, but has rotating motion like the first mode. In other words, harmful vibration to the structure of the wind-lens hardly occurs in the sandwich model until 75m/s. Most of all, its maximum displacement is far smaller than that of the other models. It is because its bending rigidity became higher by thickening the diffuser model with the use of strong CFRP laminate for the skin and light PET foam for the core. In summary, the sandwich model is considered to nearly satisfy the designed wind speed limit, 70m/s, but the reason why some peak points appeared other than 55m/s needs to be investigated.

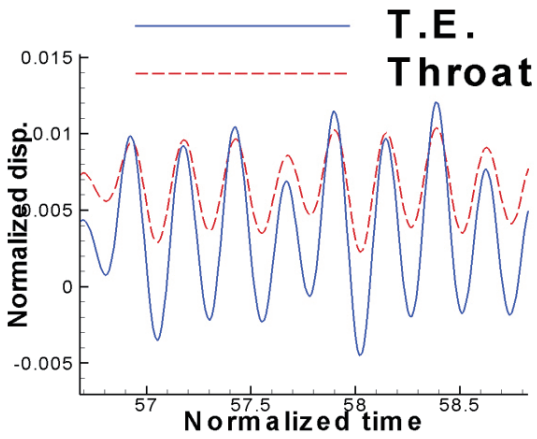

Figure 19: Time history of x-displacement at *U*=40m/s for the sandwich model

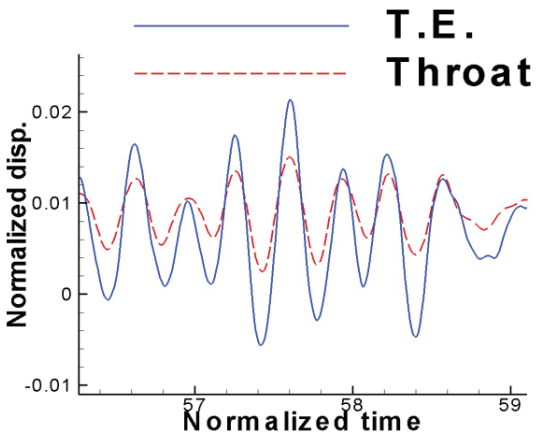

Figure 20: Time history of x-displacement at *U*=55m/s for the sandwich model

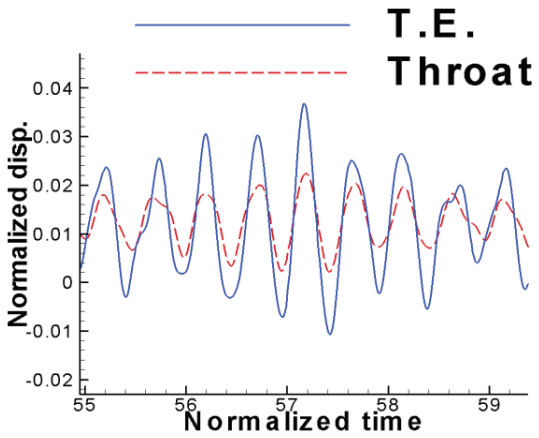

Figure 22: Time history of x-displacement at U=75m/s for the sandwich model

4. CONCLUSIONS

In this study, two-dimensional aeroelastic analysis of a brimmed-diffuser shroud for a 100kW wind power generator was conducted for the three materials: aluminum alloy, CFRP laminate and sandwich structure. We clarified that the self-excited vibration by the flow around the brimmed-diffuser shroud is amplified due to resonance when the vortex frequency is equal to the structural natural frequencies. It was also found that the dominant mode varies with wind speed. By comparing the three models under a condition of the same weight, we realized that the thickness of the model affects bending rigidity, which is relevant to the displacement of a model. In addition, we estimated the critical wind speed using the Strouhal number calculated from the rigid diffuser model, which is in good agreement with the aeroelastic responses on the whole.

REFERENCES

1) Yuji Ohya. Takashi Karasudani : A Shrouded Wind Turbine Generating High Output Power with Wind-lens Technology. Energies, 3, 2010, 634-649.
2) Yuji Ohya. Takashi Karasudani. Akira Sakurai, Ken-ichi Abe. Masahiro Inoue : Development of a shrouded wind turbine with a flanged diffuser, Journal of Wind Engineering and Industrial Aerodynamics, 96, 2008, 524-239
3) Peter Jamieson : INNOVATION IN WIND TURBINE DESIGN, John Wiley & Sons, Ltd, 2011
4) Hiroto Nagai. Koji Isogai. Tatsumi Fujimoto. Toshiyuki Hayase : Experimental and Numerical Study of Forward Flight Aerodynamics of Insect Flapping Wing, AIAA Journal, Vol. 47, No. 3, 2009, pp. 730-742
5) Hiroto Nagai. Koji Isogai. Masahiko Murozono. Tsutomu Fujishiro : Investigation on Structural and Aerodynamic Characteristics of Resonant Type Elastic Flapping Wing, ICAS2012, 2012-9.5.3, 2012